# Microstructural damage mechanics-based model for creep fracture of 9%Cr steel under prior fatigue loading

*Wei Zhang* [1,2,3], *Xiaowei Wang* [1,2,4,*], *Haofeng Chen*[3], *Tianyu Zhang* [1,2], *Jianming Gong* [1,2,*]

[1] *School of Mechanical and Power Engineering, Nanjing Tech University, Nanjing, 211816, China*

[2] *Jiangsu Key Lab of Design and Manufacture of Extreme Pressure Equipment, Nanjing, 211816, China*

[3] *Department of Mechanical and Aerospace Engineering, University of Strathclyde, Glasgow, G1 1XJ, UK*

[4] *Faculty of Engineering and Architecture, Ghent University, Zwijnaarde, B-9052, Belgium*

***Corresponding authors:**

E-mail: *xwwang@njtech.edu.cn (X. Wang)*; *gongjm@njtech.edu.cn (J. Gong)*

Tel.: +86 25 58139361; Fax: +86 25 58139361.

## ABSTRACT

Predicting the remnant creep fracture life precisely is crucial for ensuring safety of high temperature components. This study presents a microstructural damage mechanics-based model for creep fracture of 9%Cr steel under prior fatigue loading. Microstructure observation reveals that the decrease of dislocation density and the growth of martensite lath width occurred during prior fatigue process contribute to the degradation of creep strength. Particularly, coarsening of martensite lath width plays the dominated role. To take into account the effect of the prior fatigue loading, kinematic damage equations that represent the evolution of dislocation density and martensite lath are proposed in the developed model. With the proposed model, creep fracture life and creep failure strain at various lifetime factions, strain amplitudes and hold times of prior fatigue loading can be satisfactorily predicted, which manifests that the proposed model is robust in capturing the effects of various prior fatigue loadings. The proposed model is also shown to be able to accurately predict prolonged creep deformation of other similar steel after different prior fatigue loadings.

***Key words**:* Prior fatigue loading; Microstructure damage model; Creep fracture; Lath width; Dislocation density

## 1. Introduction

It is well known that in the fields of power plants and aeronautics, the creep resistance of materials is the primary concern for long-term safety operation. The creep fracture life and ductility should be deserved more attention, since they are the indispensable bases for the design and manufacture of complicated high temperature components. However, the creep fracture life and ductility can be affected by in-service operating loadings, especially the low cycle fatigue (LCF) and creep-fatigue interaction (C-F) loadings [1, 2]. Therefore, if components design is only based on original state, premature fracture may occur. Up to now, for the material in as-received state, not only a lot of experimental creep fracture data but also numerous creep models are available for high temperature component design and safety assessment [3-8]. In contrast, with regard to the material in prior fatigue state, the related studies are still limited, but, more and more researches start to focus on the influence of prior fatigue loading on subsequent creep strength [9-13]. Previous experimental studies have shown that the creep strength of Fe-Cr-Mo steels generally decreased after prior fatigue loading, which was mainly attributed to the microstructure evolution occurred during prior fatigue [10, 11, 13]. Nevertheless, note that most of the present studies evaluate the effect of prior fatigue loading on subsequent creep fracture through experimental methodology, the effective modelling approaches need to be improved.

The Auzoux's model [14] is one of the first attempts aimed at taking the prior strain effect into account to predict the subsequent creep behavior. However, since the creep strain is not coupled into the model, the Auzoux's model is rarely adapted. Recently, Erinosho et al. [15] proposed a modified crystal plasticity framework to capture the effect of dislocation glide and climb experienced during prior cyclic loading on

creep. The modified crystal plasticity model significantly promotes the development of modelling approaches for creep deformation prediction under prior fatigue loading. Meanwhile, due to the lack of directionality in terms of the accumulation of hardening [15], the crystal plasticity model is unable to account for any differences prior to stabilization. In addition, in order to consider the effect of prior LCF loading, our previous works [16] have also tried to propose a phenomenal creep model for 9%Cr steel on the basis of the Perrin-Hayhurst framework. Nevertheless, the empirical creep damage model fails to capture the microstructure damage mechanisms. The review above indicates that there are still considerable rooms for modelling approaches to be improved. In recent years, new developed Oruganti's creep model [17] did throw some light on this problem by introducing the kinetic equations that represent the transformation of microstructural features into Dyson's model [18, 19].

The present study aims to propose a comprehensive creep damage model to capture the effect of prior fatigue loading. Kinematic damage equations that represent the microstructure evolution in prior fatigue process are introduced into Oruganti's creep model. To further determine the influence of the investigated microstructure factors on modelling and to validate the observed damage mechanisms, the parameter sensitivity analysis on the proposed model is conducted. Experimental creep results at different strain amplitudes, lifetime fractions and hold times of prior fatigue loading are utilized to validate the accuracy and the predictive capacity of the proposed model. Long-term creep data of other similar steel is also employed to verify the reliability of the proposed model.

## 2. Experiments

### *2.1. Experimental procedures*

Detailed experimental procedures and results have been reported in our previous works [13, 16, 20], therefore, to avoid a repeated description, only the main experimental procedures and results are presented in

the current work. The schematic representation of the experimental procedures is presented in Fig. 1, which consists of fatigue lifetime determination test, prior fatigue test and final creep fracture test. The material utilized in the experiments is P92 steel. Strain amplitudes of 0.25% and 0.4% were imposed on LCF tests. Tensile hold time ranging from 0 s to 600 s at 0.4% strain amplitude was imposed on C-F tests. All the LCF and C-F tests were performed under total strain control with a constant strain rate of $1\times10^{-3}$ $s^{-1}$ at 650 °C. Creep tests were conducted till fracture at creep load of 130 MPa and at 650 °C. During all the tests, the temperature was controlled within ±2 °C. Detailed test conditions and data are summarized and listed in Table 1. Transmission electron microscopy (TEM) observation on specimens after prior fatigue loading and subsequent creep loading were also conducted by using a JEOL JEM-2010 instrument. Martensite lath width was measured from the TEM micrographs through the linear intercept method. The final martensite lath width presented in the current study was averaged from at least twenty measurements as listed in Table 1.

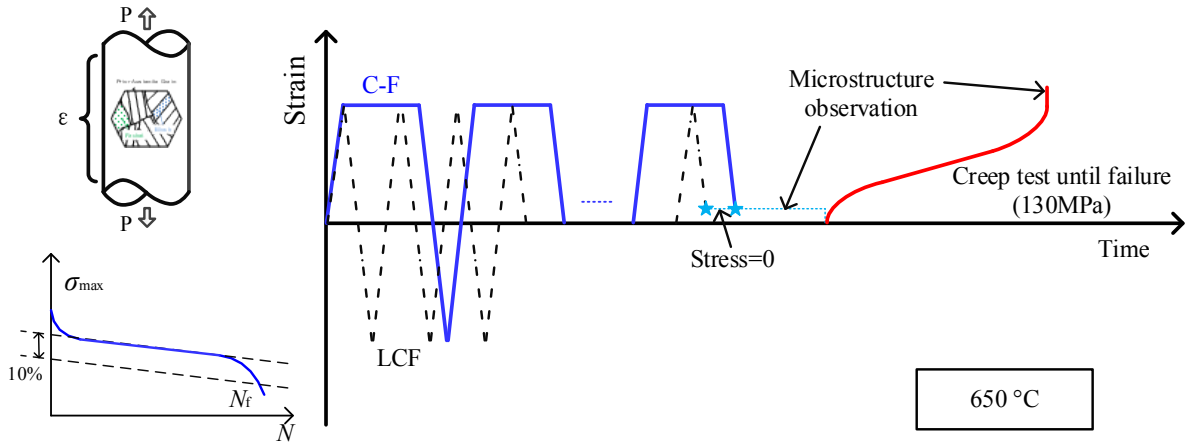


Fig. 1. Schematic representation of experimental procedures

Table 1 Test conditions and results of prior fatigue loading and subsequent creep tests at 650 °C

| Test No. | Load pattern | Strain amplitude (%) | Hold time (s) | Lifetime fraction | Martensite lath width (μm) | Experimental creep fracture life (h) | Predicted creep fracture life (h) |
|---|---|---|---|---|---|---|---|
| 1 | | As-received state | | | 0.375 | 1143 | 1146 |
| 2 | LCF | 0.25 | / | 20% | 0.58 | 1085 | 1039 |
| 3 | LCF | 0.25 | / | 50% | 0.9 | 747 | 695 |
| 4 | LCF | 0.25 | / | 70% | 1.2 | 512 | 489 |
| 5 | LCF | 0.25 | / | 80% | 1.24 | 509 | 468 |
| 6 | LCF | 0.4 | / | 10% | 0.54 | 1094 | 1089 |
| 7 | LCF | 0.4 | / | 20% | 0.766 | 864 | 820 |
| 8 | LCF | 0.4 | / | 50% | 1.1 | 540 | 550 |
| 9 | LCF | 0.4 | / | 70% | 1.25 | 503 | 463 |
| 10 | C-F | 0.4 | 180 | 10% | 0.46 | 1082 | 1076 |
| 11 | C-F | 0.4 | 180 | 20% | 0.66 | 921 | 940 |
| 12 | C-F | 0.4 | 180 | 50% | 1.1 | 129 | 550 |
| 13 | C-F | 0.4 | 180 | 70% | 1.22 | 186 | 479 |
| 14 | C-F | 0.4 | 30 | 20% | 0.755 | 833 | 832 |
| 15 | C-F | 0.4 | 600 | 20% | 0.775 | 892 | 810 |

*2.2. Experimental results*

Experimental results have revealed that remnant creep properties of P92 steel varied a lot with respect to lifetime fraction, strain amplitude and hold time of prior fatigue loading [13, 16, 20]. The higher lifetime fraction and strain amplitude the more catastrophic degradation of remnant creep strength was noticed. Nevertheless, the variation of hold time hardly alters the subsequent creep strength. The obvious recovery of microstructures in fatigue process has been demonstrated to be responsible for these phenomena [21], as typically shown in Fig. 2. During fatigue process, the decrease of dislocation density and the martensite lath recovery take place, as pointed by red arrow and blue arrow in Fig. 2, respectively. However, no evident coarsening of precipitates occurs in prior fatigue process as pointed by yellow arrow in Fig. 2, therefore, its effect on subsequent creep fracture will be neglected in the following proposed model. The detailed microstructure damage mechanisms are schematically illustrated in Fig. 3. According to these damage

philosophies, a microstructural damage mechanics-based model for creep fracture of 9%Cr steel under prior fatigue loading will be proposed.

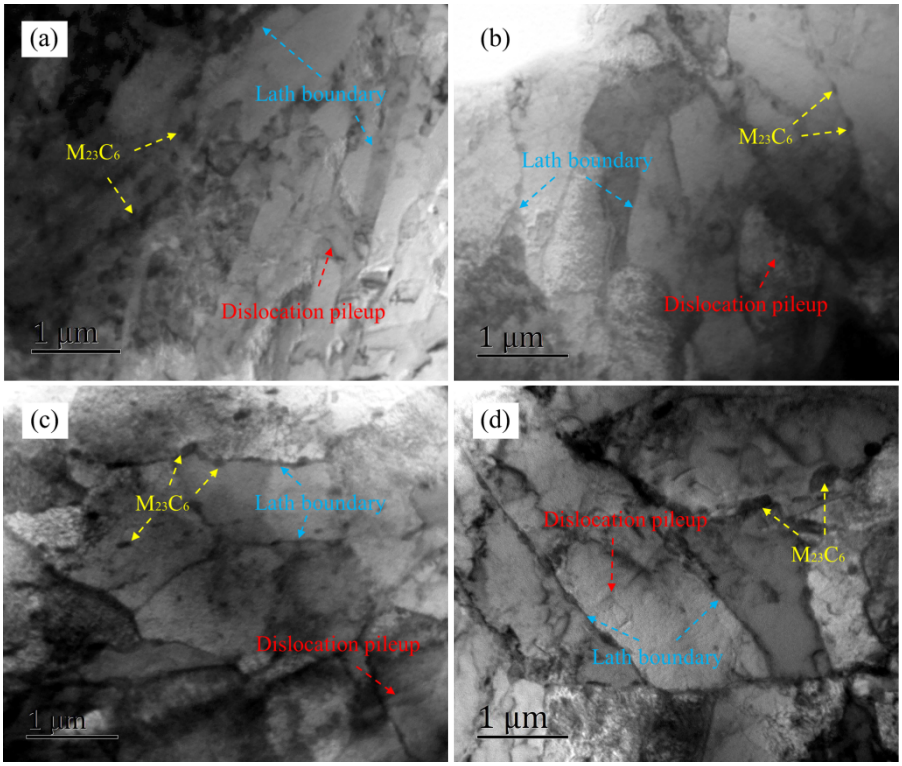


Fig. 2. TEM micrographs of specimens at various prior fatigue loadings: (a) as-received, (b) 20% lifetime fraction of 0.4% prior LCF, (c) 50% lifetime fraction of 0.4% prior LCF, (d) 20% lifetime fraction of 180s prior C-F

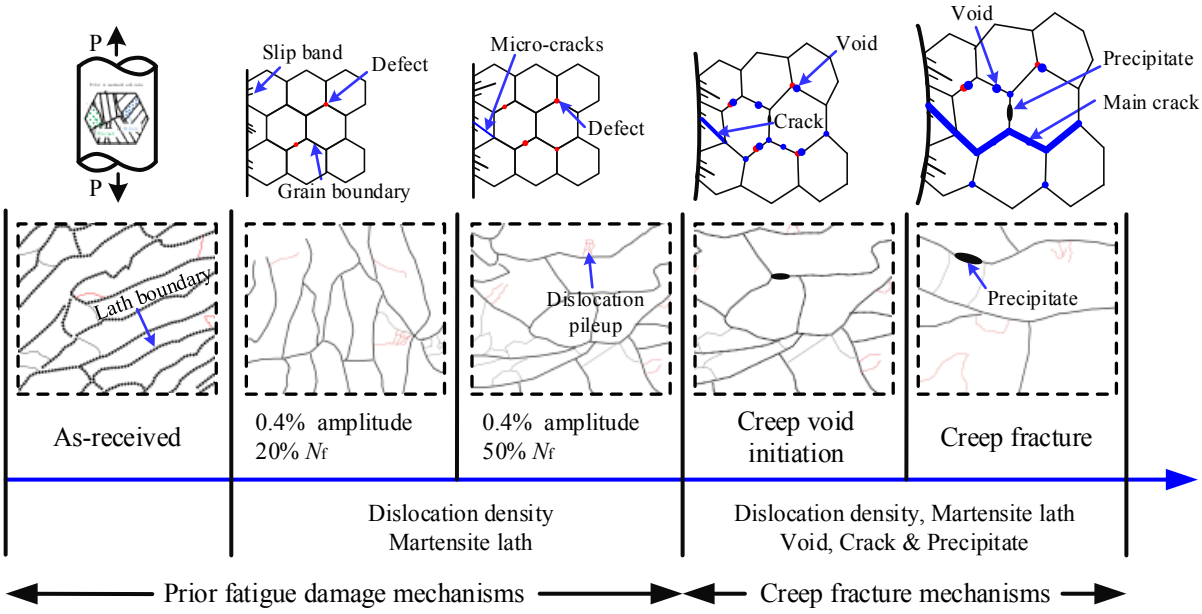


Fig. 3. Schematic of microscopic damage mechanisms in the prior fatigue and subsequent creep processes

## 3. Fundamental creep model

Oruganti's creep model was developed within the continuum damage mechanics (CDM) framework described by Dyson [18, 19]. In Oruganti's model, the evolution of carbonitrides and subgrain with time and strain was described through two kinetic equations, which make it capable of predicting creep data up to tens of thousands of hours. In addition, Oruganti considered the back stress to decrease with increasing the subgrain width due to stress redistribution between grains walls and grain interiors [22], and Oruganti also considered that the initial dislocation structure contributes to the significant primary strain accumulation. The novel creep damage model particularly provides a better method to capture the effect of prior fatigue loading. The fundamental equation in Oruganti's creep model without considering temperature effect is given as [17]:

Master equation
$$\dot{\varepsilon} = \dot{\varepsilon}_0' \sinh\left[\frac{\sigma - \sigma_B}{\sigma_o\left(1 - D_P\right)}\right] \tag{1}$$

$$\sigma_B = H^*\left(1 - D_S\right) \tag{2}$$

Primary creep
$$\dot{\sigma}_o = K_1\left(1 - \frac{\sigma_o}{K_2}\right)\dot{\varepsilon} \tag{3}$$

Subgrain evolution
$$\dot{D}_S = \frac{K_S}{S_i}\left(1 - D_S\right)^2 \dot{\varepsilon} \tag{4}$$

Precipitate evolution
$$\dot{D}_P = \frac{K_P}{3}\left(1 - D_P\right)^4 \tag{5}$$

where $\dot{\varepsilon}_0'$, $K_S$ are material constants, $H^*$ is the saturated value of hardening state variable, $\sigma_o$ is the reference stress, $K_1$ is the evolution rate of reference stress, $K_2$ is the saturated value of reference stress and $K_P$ is ageing parameter, $\sigma_B$ is the back stress that is supposed to arise due to aforementioned stress redistribution between grains walls and grain interiors. Eq. (3) indicates that reference stress $\sigma_o$ would increase at a rate of $K_1$ and reach a saturated value of $K_2$ until the end of primary creep stage. Since

Oruganti's creep model has considered the effect of initial subgrain size on creep deformation, its ability to capture effect of prior fatigue loading is also presented for comparison.

## 4. Proposed creep damage model

### *4.1 Decline of dislocation density*

The martensitic microstructure of 9%Cr steel generally possesses high dislocation density after the normalizing and tempering process [23, 24], as shown in Fig. 2(a). Presence of high dislocation density results in a large driving force required for recovery, which produces a stable structure as required for hjgh creep resistance [25, 26]. Nevertheless, the high dislocation density drops rapidly in very small strain intervals of primary creep stage [26, 27]. This in turn causes evident creep strain accumulation, especially at no prior fatigue state, as shown in Fig. 4 (black line). However, note that the creep strain accumulation in primary stage decreases after prior fatigue loading (Fig. 4). One possible explanation could be that the initial stable dislocation structure may not be in equilibrium with the applied stress [17]. As the applied stress is same in the present study, there is no doubt that the decline of dislocation density observed during prior fatigue process, as shown in Figs. 2 and 3, accounts for the phenomenon. This result is important in view of the object of the proposed model. In Oruganti's model, primary creep equation (Eq. (3)) was developed to describe the strain accumulation. Since the prior fatigue loading only accelerates the creep damage rather than alters the material inherent creep properties, the unchanged steady value of $K_2$ in Eq. (3) can be assumed. Consequently, reference stress rate (strain accumulation rate) dependent parameter $K_1$ should be modified according to the effect of decrease of dislocation density. Base on the dislocation density at as-received and after prior fatigue loading, a damage parameter $D_d$ is defined as follows:

$$D_d = \frac{\rho}{\rho_0} \tag{6}$$

where $\rho_0$ is dislocation density at as-received condition, $\rho$ is dislocation density after prior fatigue loading, which is dependent on prior fatigue loading. Note that the damage parameter $0<D_d\leqslant 1$ and decreases with the decline of dislocation density after prior fatigue loading. The effect of decrease of dislocation density during prior fatigue loading can then be accounted by dividing $K_1$ in the creep equation by $D_d$. Consequently, the kinematic damage equation for the decrease of dislocation density can be obtained as:

$$\dot{\sigma}_o = \frac{K_1}{D_d}\left(1-\frac{\sigma_o}{K_2}\right)\dot{\varepsilon} \tag{7}$$

For 9%Cr steel, the dislocation density at as-received condition $\rho_0$ is about $1.6\times10^{14}$ $m^{-2}$ [28-31]. Unfortunately, because of the limited access to measure the dislocation density in the current work and so far few conferences report dislocation data during fatigue process, therefore the equation proposed by Leen et al. [32] for the simulation of dislocation density of 9%Cr steel during fatigue loading is adopted here to obtain the value of $\rho$, which is listed below:

$$\rho = \vec{\rho} + f_i\rho_i + f_w\rho_w + f_g\rho_g \tag{8}$$

where $\vec{\rho}$ is mobile dislocation density, $f_j$ (j=i, w, g) is volume fraction, the subscripts i, w and g denotes lath interior, low angle boundary (LAB) and high angle grain boundary (HAGB), respectively, $\rho_j$ (j=i, w, g) is dislocation density corresponding to various volume fractions. The evolution of dislocation density of 9%Cr steel at various fatigue loading conditions can be acquired through the equation with the same parameters listed in Ref. [32]. Fig. 5 depicts the predicted evolution of dislocation density by the Leen's model. It can be seen the Leen's model can give a good description for variation of dislocation density at both LCF and C-F loadings. However, it is also noteworthy that only few experimental data were used to verify the accuracy of the evolution of dislocation density, its reliability still needs more experimental results to validate.

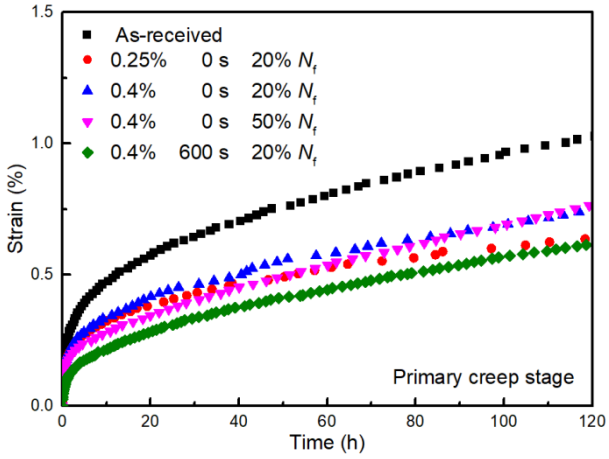


Fig. 4. Experimental primary creep curves at various prior fatigue loading conditions

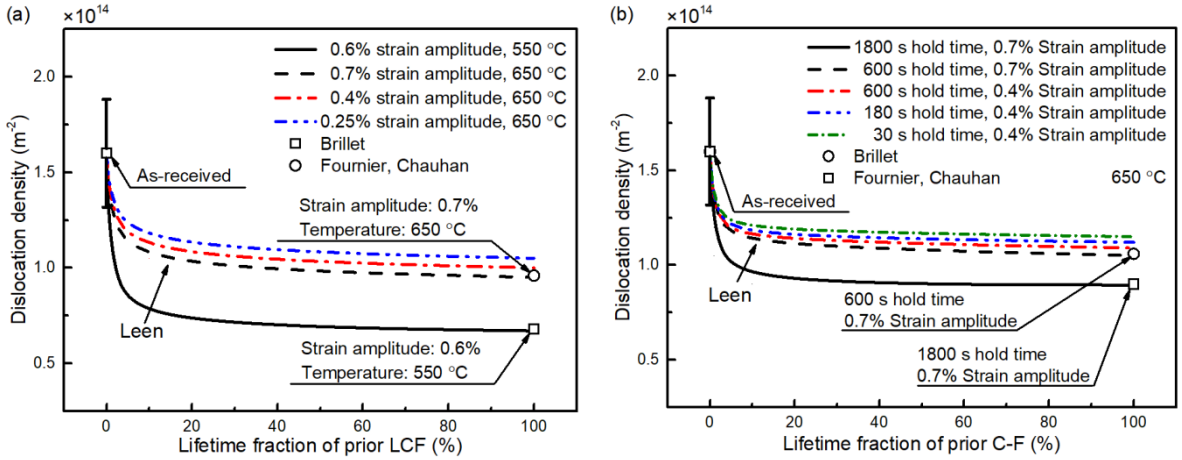


Fig. 5. Evolution of dislocation density at (a) different lifetime fractions of LCF loading and (b) different lifetime fractions of C-F loading [28-35]

*4.2 Martensite lath recovery*

Apart from the dislocation strengthening, the lath (sub)boundary strengthening is an another main factor that governs the creep strength of 9%Cr steel [36]. The lath (sub)boundary acts as obstacles against dislocation motion during creep deformation, and the lath (sub)boundary strengthening has been reported to much greater than the precipitates strengthening [ 37]. However, the lath width was observed to be increased during creep process that lead to the degradation of creep strength [38]. Hence, the martensite lath recovery occurred during prior fatigue loading, as presented in Figs. 2 and 3, definitely accelerates the reduction of

creep strength. Barrett el al. [39, 40] reported that loss of lath (sub)boundary strengthening resulted in a decrease of back stress, $\sigma_B$. In Oruganti's model, the evolution of back stress caused by subgrain growth had been considered. Since the strengthening from subgrain boundaries is same as the lath boundary strengthening [41], therefore the effect of the recovery of martensite lath width during prior fatigue loading can be evaluated through the back stress. As a consequence, the back stress in Eq. (2) can be rewritten as:

$$\sigma_{B=}\sigma H^{*}(1\text{-}D_L) \tag{9}$$

where $D_L$ is damage parameter for martensite lath recovery. As similar to the damage evolution of subgrain growth, the following equation was utilized to represent the damage evolution of martensite lath recovery:

$$\dot{D}_L = \frac{K_L}{L_i}\left(1-D_L\right)^2 \dot{\varepsilon} \tag{10}$$

where $K_L$ is material constant, $L_i$ is the martensite lath width after prior fatigue loading. The martensite lath width at various lifetime fractions, strain amplitudes and hold times prior fatigue loading measured through the linear intercept method is shown in Fig. 6 and listed in Table 1. It is observed that the increase in lifetime fraction and strain amplitude induces evident coarsening of martensite lath width. Regarding the effect of hold time, the martensite lath width was found to be little altered even though hold period of prior C-F loading increases.

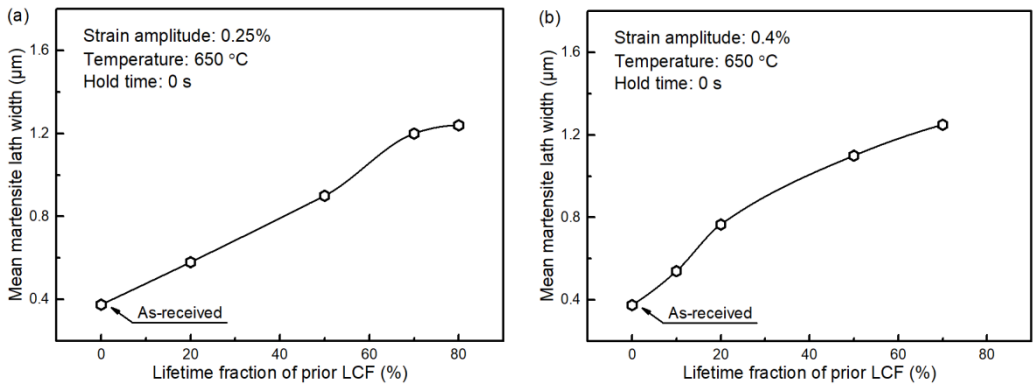

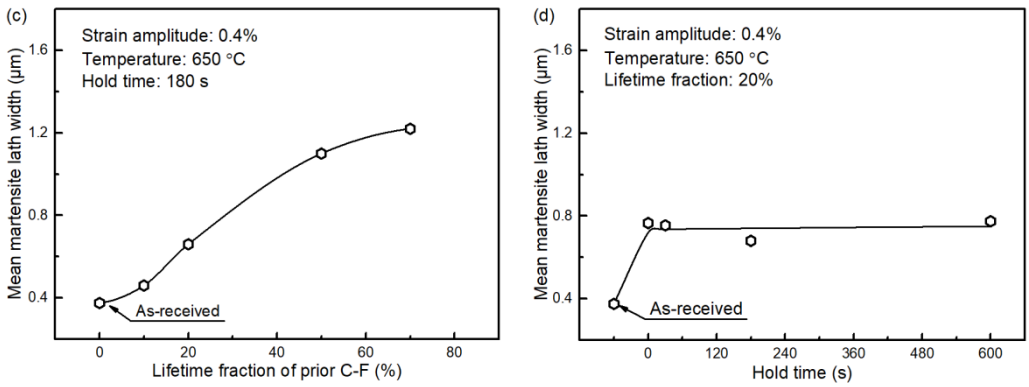


Fig. 6. Evolution of martensite lath width at various prior fatigue loading conditions: (a) 0.25% strain amplitude prior LCF loading, (b) 0.4% strain amplitude prior LCF loading, (c) 180 s hold time prior C-F loading, (d) 20% lifetime fraction prior C-F loading

*4.3 Creep void evolution*

The grain boundary cavitation is known widely to result in the final creep fracture in high temperature components [42, 43]. The nucleation and growth of cavities (void of boundaries), coalescence of neighboring cavities leading to the formation of microcracks, which can then link-up with the macroscopic crack primarily, contribute to the creep fracture [44], as illustrated in Fig. 3. Nevertheless, it has been revealed that the motion of slip bands which is a considerable reason for the recovery of martensite lath [45] could convey some defects, i.e. vacancies, to the lath boundaries, promoting the nucleation of creep cavities and facilitating growth of microcracks and the final fracture, as presented in Fig. 3. Therefore, the effect of creep void evolution and the additional effect caused by prior fatigue loading should be taken into account. Based on the approach developed for the inter-granular creep constrained void damage by Hayhurst et al. [46, 47], the following expression for the damage evolution of creep void after prior fatigue loading is defined:

$$\dot{D}_{\mathrm{N}} = \frac{K_{\mathrm{N}}}{\varepsilon_{\mathrm{f}}}\dot{\varepsilon} + D_{\mathrm{F}}\dot{\varepsilon} \tag{11}$$

where $D_N$ is damage parameter for creep void, the item $\frac{K_N}{\varepsilon_f}\dot{\varepsilon}$ is the conventional damage equation for creep void, $K_N$ is the damage value at fracture, $K_N$=1/3 is adopted here [47], $\varepsilon_f$ is the uniaxial failure strain, the item $D_F\dot{\varepsilon}$ is the modified creep void damage, which was proposed to consider the additional effect of prior fatigue loading. Since the creep void initiates along lath boundaries [48], $D_F$ is therefore reasonable to be assessed with the martensite lath width and given as follows:

$$D_F=f(L) \tag{12}$$

Considering that the more recovery of martensite lath width the more defects are generated, the damage $D_F$ is hereby evaluated based on the initial and current martensite lath width and given as follows:

$$D_F=A*(L_i-L_0) \tag{13}$$

where $A$ is material constant, $L_0$ is the martensite lath width at as-received state.

*4.4. Assumptions of the proposed model*

Coarsening of precipitates is a phenomenon that results in significant loss in creep strength and it is strongly dependent on time. However, in the current work no evident coarsening of precipitates happened during prior fatigue process (Figs. 2 and 3) due to the short prior fatigue test period, which is in consistent with works by Gopinath et al. [49] and Xuan et al. [50]. Consequently, the coarsening of precipitates was being ignored here, nevertheless, this will be verified by the parameter sensitivity analysis in Section 5.2.

*4.5. Final creep damage model*

The proposed final creep damage equation set for capturing prior fatigue loading effect of the 9%Cr steel is as follows.

Master equation
$$\dot{\varepsilon}=\dot{\varepsilon}_0'\sinh\left[\frac{\sigma-\sigma_B}{\sigma_o(1-D_P)(1-D_N)}\right] \tag{14}$$

$$\sigma_B=H^*(1-D_L) \tag{15}$$

Primary creep $$\dot{\sigma}_o = \frac{K_1}{D_d}\left(1 - \frac{\sigma_o}{K_2}\right)\dot{\varepsilon} \quad (16)$$

$$D_d = \frac{\rho}{\rho_0} \quad (17)$$

Martensite lath evolution $$\dot{D}_L = \frac{K_L}{L_i}(1 - D_L)^2\,\dot{\varepsilon} \quad (18)$$

Precipitate evolution $$\dot{D}_P = \frac{K_P}{3}(1 - D_P)^4 \quad (19)$$

Creep void evolution $$\dot{D}_N = \frac{K_N}{\varepsilon_f}\dot{\varepsilon} + D_F\dot{\varepsilon} \quad (20)$$

$$D_F = A^*(L_i - L_0) \quad (21)$$

## 5. Simulation results and discussion

### *5.1. Determination of parameters*

Experimental creep results at 140 MPa, 130 MPa and 125 MPa of 650 °C were used to determine the model parameters of the as-received specimen. The optimization program is implemented in Matlab software with a gradient-based Levenberg-Marquardt algorithm, which aims to seek the minimum differences between experimental and simulated results. In the as-received condition, the prior fatigue damage was set as 'zero', where $\rho=\rho_0=1.6\times10^{14}$ m$^{-2}$ and $L_i=L_0=0.375$ μm. The entire determination procedure is detailed as follows: (1) fixing the initial value of $\sigma_0$ at 3 MPa arbitrarily; (2) the aforementioned optimization procedures were used to determine the value of $\dot{\varepsilon}_0'$, $K_1$ and $K_2$: the value of $\dot{\varepsilon}_0'$ was determined from the data of logarithm of the minimum creep rate versus the logarithm of stress; $K_1$ is located within the range of shear modulus; $K_2$ is the saturated value of $\sigma_0$; The creep curves before 100 h were used in optimization procedure here; (3) by fixing $\dot{\varepsilon}_0'$, $K_1$, $K_2$, $\varepsilon_f$ ($\varepsilon_f$ = 0.2 from experimental data shown in Fig. 7) and $H^*$ ($H^*$ =0.45 [17]), the values of $K_L$ and $K_P$ were determined through fitting experimental data; (4) finally, all the previous determined material parameters were optimized again by employing the experimental creep curves. The

optimum material parameters in the proposed model are finally identified and listed in Table 2. Creep test of 120 MPa at 650 °C was carried out to verify the determined material parameters. Fig. 7 presents the comparison of predicted and experimental creep curves at various creep loadings. It is observed that the proposed model with the determined parameters gives satisfactory reproduction of creep deformation for all loading conditions of 140 MPa, 130 MPa, 125 MPa and 120 MPa. Moreover, the proposed model also presents a comparable predictive capacity at long-term creep tests up to tens of thousands of hours which data are available [33].

Table 2 Parameters of the proposed model for 9%Cr steel at 650 °C

| Parameters | $\dot{\varepsilon}_0'$ ($h^{-1}$) | $K_1$(MPa) | $K_2$(MPa) | $H^*$(-) | $K_L$($h^{-1}$) | $K_P$($h^{-1}$) | $K_N$(-) | $A$(-) |
|---|---|---|---|---|---|---|---|---|
| Values | $8\times10^{-10}$ | 2400 | 6.2 | 0.5 | 1 | $1.5\times10^{-5}$ | 0.3 | 6.418 |

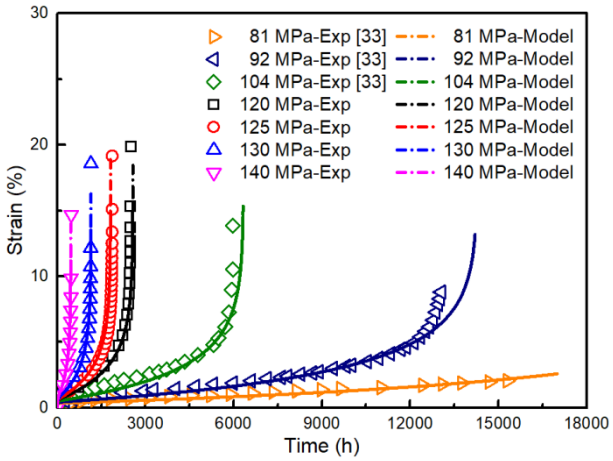


Fig. 7. Experimental and predicted creep curves at various creep loadings

After the determination of material parameters for as-received condition, it is necessary to determine the prior fatigue loading related parameters. Since the martensite lath width has been measured from our experimental results and the evolution of dislocation density can also be determined through Eq. (8), the parameter $A$ is becoming the only parameter needed to be determined here. By fitting the creep results after 0.4% strain amplitude prior LCF loading, as depicted in Fig. 9, it is easy to get the parameter $A$, as listed in

Table 2. It is worth noting that only the experimental results at various lifetime fractions of 0.4% strain amplitude prior LCF loading were used to obtain these material parameters.

*5.2. Parameter sensitivity analysis*

To further illustrate the influence of the investigated microstructure factors on modelling and to validate the damage mechanisms observed in the current study, the sensitivity analysis on the proposed model was performed in this section. The investigated microstructure factors include strain accumulation rate dependent parameter $K_1$, initial martensite lath width related parameter $K_L$, creep void parameter related to the martensite lath recovery $A$, and precipitate evolution related aging parameter $K_P$. The effects of various values of parameters mentioned above on creep curves are presented in Fig. 8. Experimental creep curve at 10% lifetime fraction of 0.4% strain amplitude prior LCF loading is selected as example here to conduct sensitivity analysis. From Fig. 8, it can be seen that the proposed model is the most sensitive to the martensite lath width related parameters $K_L$ and $A$, which indicates that the coarsening of martensite lath width occurred in prior fatigue process plays the dominant role in degradation of subsequent creep strength. In contrast, the other two remaining parameters shows lower sensitivity behaviors, especially the precipitate evolution related aging parameter $K_P$. This also proves the assumptions mentioned in Section 4.4 is reasonable.

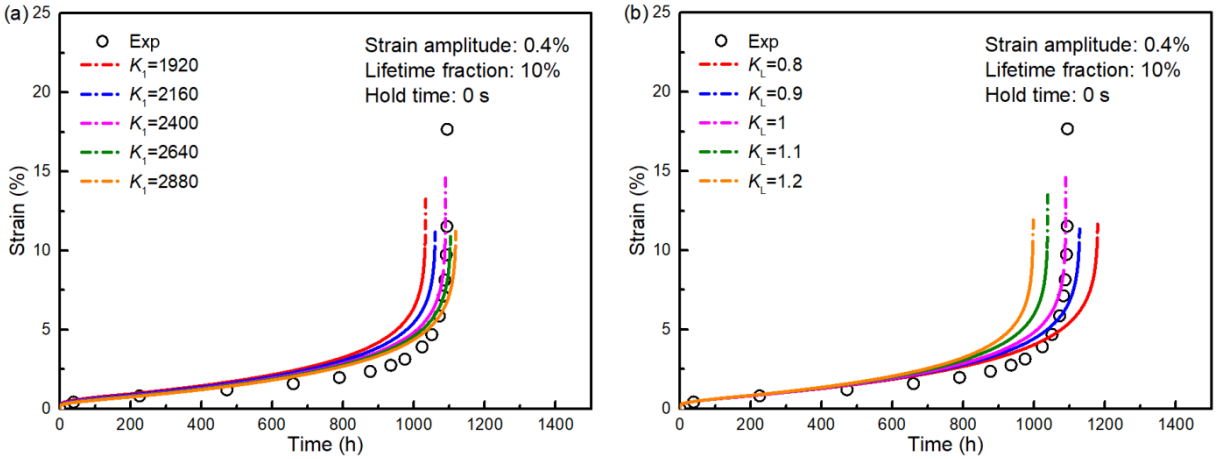

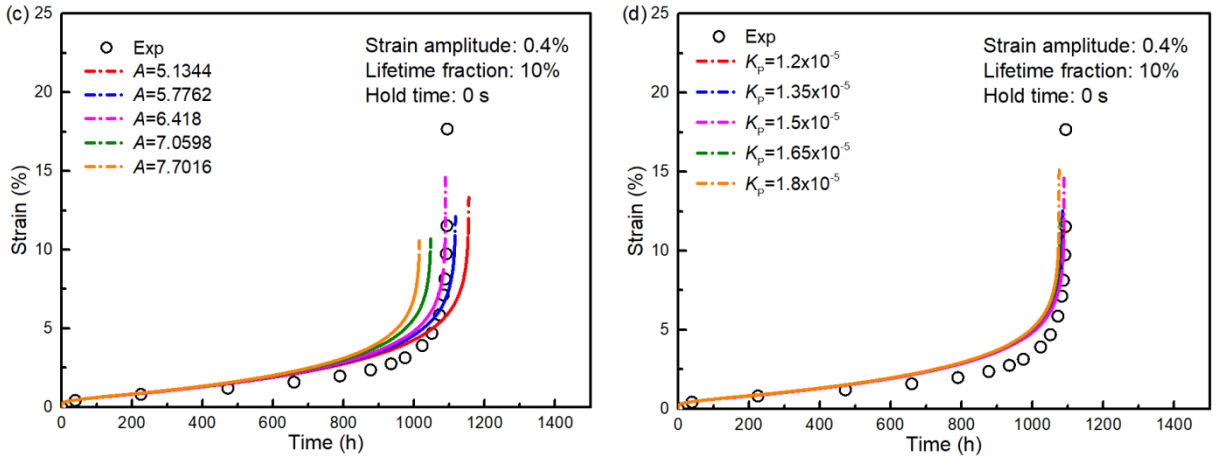


Fig. 8. Comparison of creep curves at various parameters (a) $K_1$, (b) $K_L$, (c) $A$, (d) $K_P$

*5.3. Validation of model accuracy*

To validate the accuracy of the proposed model, experimental and simulated results are compared, as presented in Fig. 9. The simulated results calculated by Oruganti's model are also presented for comparison. Experimental data, which are utilized to determine model parameter $A$, are used here. Fig. 9(a) indicates that the proposed model can satisfactorily describe the creep deformation after various prior fatigue loadings. However, although Oruganti's model can give a comparable simulation at as-received condition, Oruganti's model fails to simulate the creep curves after prior fatigue loadings due to the absence of consideration on prior fatigue loading effect. It is also worth noting that the creep primary stage is well reproduced by the proposed model, as shown in Fig. 9(b), which suggests that the proposed model can reasonably capture the effect of decline of dislocation density.

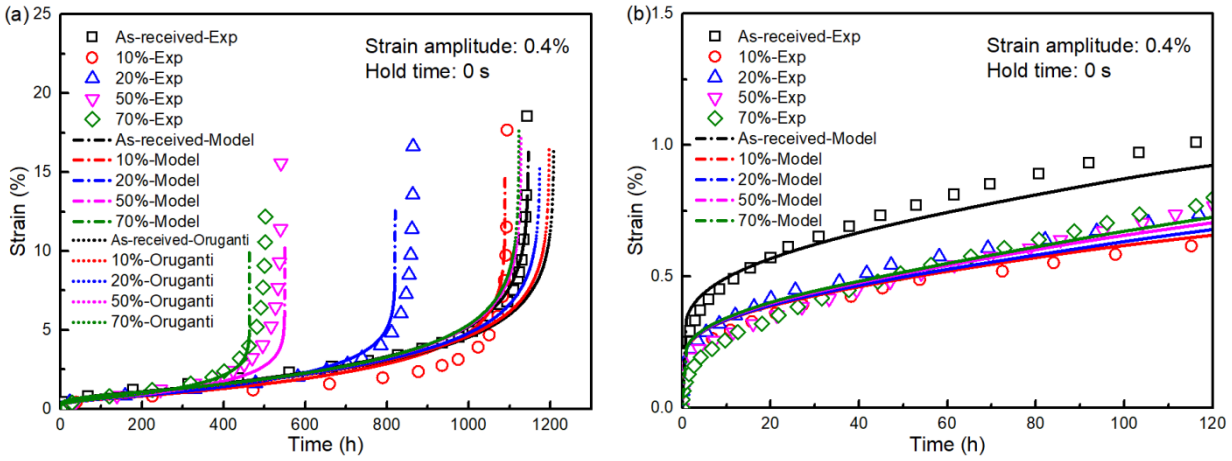


Fig. 9. Comparison of experimental creep curves (a) and creep primary stage (b) with predicted creep curves at different lifetime fractions of 0.4% strain amplitude prior LCF loading

In addition to the creep deformation, the creep fracture life and creep ductility need to be further validated as well, because they are important bases for the safety assessment and components design [51, 52]. The comparison of creep fracture life and creep ductility between experimental and simulated results under different lifetime fractions of 0.4% strain amplitude prior LCF loading are plotted in Fig. 10(a) and (b) (blue circle), respectively. The predicted creep fracture life and creep failure strain were determined from the last point of the simulated creep curve, where creep rate reaches infinite. It is shown that the proposed creep damage model gives a good prediction for creep fracture life and creep failure strain under 0.4% strain amplitude prior LCF loading. In contrast, the predicted creep fracture life of Oruganti's model dramatically diverges from the experimental creep data. Particularly, note that the experimental results simulated here were used for the determination of material parameters, predictive capacity of the proposed model are thus needed to be evaluated.

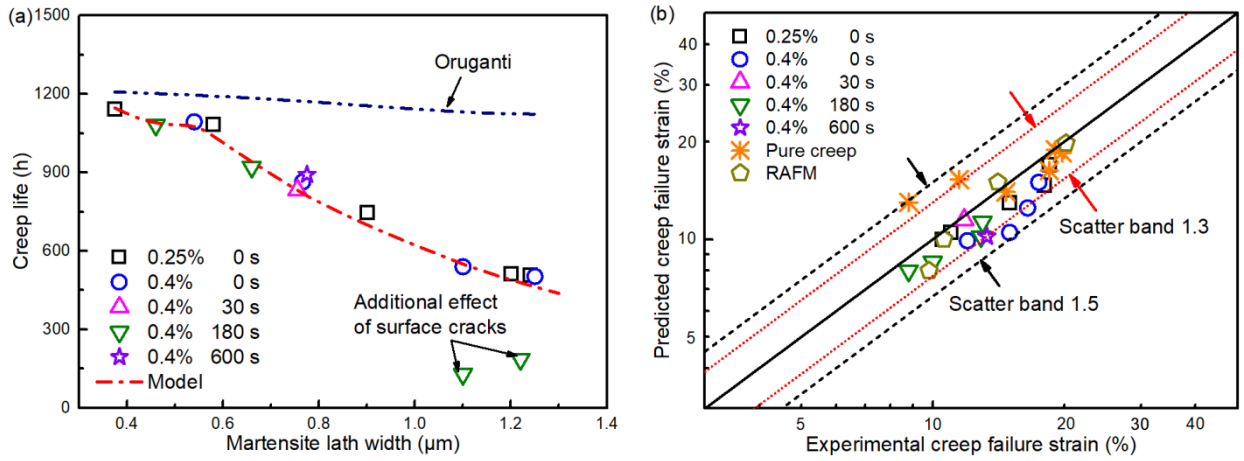


Fig. 10. (a) Comparison of predicted and experimental creep fracture life and (b) comparison of predicted and experimental creep failure strain

*5.4. Predictive capability of the proposed model*

The objective of this section is to evaluate the predictive capability of the proposed model. On the one hand, the capability of the proposed model to predict the experimental results at different strain amplitudes and different hold times of prior fatigue loading will be assessed. These experimental data are not used during the determination of material parameters. On the other hand, the capability of the proposed model to predict other long-term tests of similar materials will be evaluated.

Fig. 11(a), (b) and (c) display the predicted results of creep curves at different lifetime fractions of 0.25% strain amplitude prior LCF loading, different lifetime fractions of 180 s hold time prior C-F loading, and 20% lifetime fraction of different hold times prior C-F loading, respectively. These predicted results were obtained without any fitting procedure. The good agreement between predicted and experimental results demonstrates that the proposed model can be directly extended to other strain amplitudes and hold times of prior fatigue loading. However, it is worth noting that the proposed model underestimates the damages of 50% and 70% lifetime fraction of 180 s hold time prior C-F loading. This is because as the lifetime fraction of prior C-F loading increases further, apart from the recovery of microstructures, the evident growth of surface

cracks takes place [20]. The surface cracks will introduce additional damage on subsequent creep strength and the damage mechanism of prior C-F loading transforms to the combined effect of microstructure evolution and obvious surface cracks.

To further verify the accuracy of the proposed model at various strain amplitudes and various hold times of prior fatigue loading, creep fracture life and creep ductility were compared, as depicted in Fig. 10. The creep ductility of various creep stress tests (Fig. 7) is also presented for comparison. It is observed that except the 50% and 70% lifetime fraction of 180 s hold time prior C-F loading as mentioned above, the proposed model can give an accurate prediction for remnant creep fracture life, as shown in Fig. 10(a). Hence it validates the robustness of the proposed model to capture the effect of various prior fatigue loadings on creep fracture life. Regarding the creep failure strain, in comparison with experimental data, all the predicted creep failure strains at different prior fatigue loadings and different creep stresses locate within a scatter band of 1.5, as shown in Fig. 10(b). Consequently, the proposed model is proved to be capable of predicting the stress dependent failure strain. Further observation of Fig. 10(b) reveals that most of the predicted results fall into a scatter band of 1.3. The other points whose experimental data mainly come from reference fall out the 1.3 band. The higher scatter of those points may thus be ascribed to the different batches of materials [53]. Although the proposed model has been proved to predict the experimental results reasonably, it still needs further validation in the future by using a wide range of the experimental database, which could give more support to its industrial applicability.

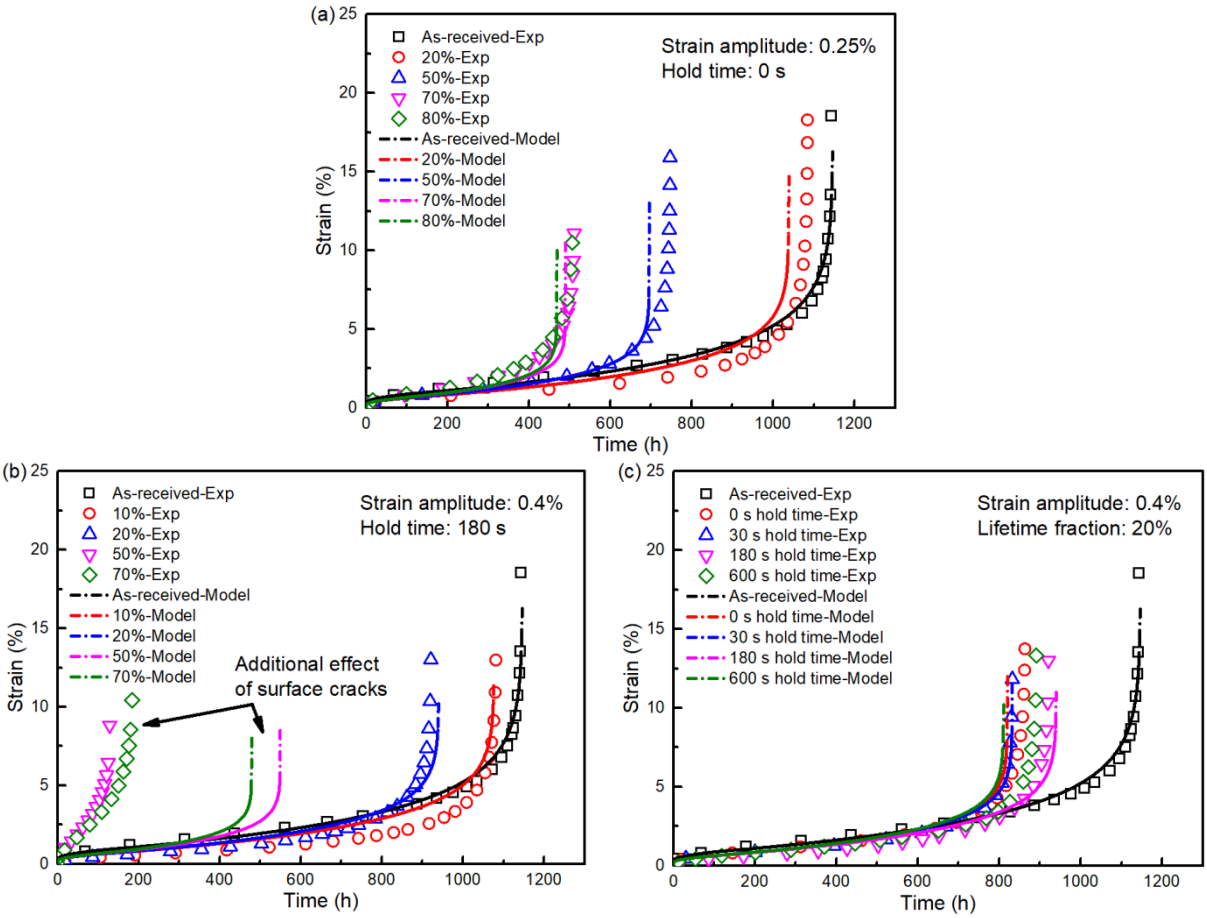


Fig. 11. Comparison of experimental creep curves and predicted creep curves at various prior fatigue loading conditions: (a) 0.25% strain amplitude prior LCF loading, (b) 180 s hold time prior C-F loading, (c) 20% lifetime fraction prior C-F loading

The capability of the proposed model to predict long-term creep deformation of other similar steel under prior fatigue loading should be validated as well. Creep data of reduced activation ferritic-martensitic (RAFM) steel were employed here [10]. During the validation process, the material parameters for RAFM steel at 550 °C were recalculated through the method discussed above and are listed in Table 3. Fig. 12 compares the predicted results of RAFM steel with the experimental data. It can be seen that the proposed model can be extended to predict long-term creep fracture life accurately up to nine thousand hours at different temperatures. Moreover, the creep curves and creep ductility (Fig. 10(b)) of RAFM steel after prior

fatigue loadings can be well described as well, which indicates that the effect of various prior fatigue loadings at different strain rates and temperatures can be reproduced using the proposed model.

Table 3 Parameters of the proposed model for RAFM steel at 550 °C

| Parameters | $\dot{\varepsilon}_0'$ ($h^{-1}$) | $K_1$(MPa) | $K_2$(MPa) | $H^*$(-) | $K_L$($h^{-1}$) | $K_P$($h^{-1}$) | $K_N$(-) | $A$(-) |
|---|---|---|---|---|---|---|---|---|
| Values | $1\times10^{-11}$ | 1250 | 9.5 | 0.45 | 1 | $1.5\times10^{-5}$ | 0.3 | 30 |

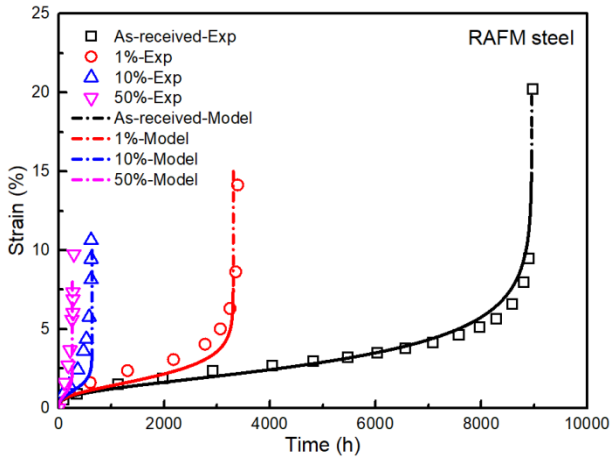


Fig. 12. Comparison of experimental creep curves and predicted creep curves of RAFM steel under prior LCF loadings (Prior LCF: strain amplitude of 0.6%, strain rate of $1\times10^{-3}$ $s^{-1}$, temperature of 550 °C; Creep: creep load of 210 MPa, temperature of 550 °C) [10]

## 6. Summary and Conclusions

The coarsening of martensite lath width occurred during prior fatigue process plays the dominant role in degradation of subsequent creep strength. By incorporating the effect of decrease of dislocation density on strain accumulation, recovery of martensite lath on stress redistribution and its corresponding influence on creep void evolution, the proposed creep model gives a satisfactory prediction for creep deformation at various prior fatigue loadings. Not only the creep fracture life but also the creep failure strain can be well

described by the proposed model. Moreover, the proposed creep damage model can also be directly extended to other similar steel and long-term creep test.

## Acknowledgements

The authors gratefully acknowledge the financial support of the National Key R&D Program of China (No. 2018YFC0808800), China Postdoctoral Science Foundation (No. 2016M600405) and innovation program for graduate students in Jiangsu Province of China (No. KYCX17_0935). We also thank Mr. Yinong Lyu from School of Material Science and Engineering, Nanjing Tech University, for his help with the TEM specimens' preparation and observation and the support from China Scholarship Council (CSC) and the University of Strathclyde.

## References

[1] Chaudhuri S, Ghosh RN. Creep behavior of 2.25 Cr1Mo steel-Effects of thermal ageing and pre-strain. Mater Sci Eng, A 2009;510:136-141.
[2] Zhang XC, Tu ST, Xuan FZ. Creep–fatigue endurance of 304 stainless steels. Theor Appl Fract Mech 2014;71:51-66.
[3] Song K, Zhao L, Xu LY, Han YD, Jing HY. Experimental and numerical analysis of creep and damage behavior of P92 steel by small punch tests. Theor Appl Fract Mech 2019:100;181-190.
[4] Hayhurst DR, Dimmer PR, Morrison CJ. Development of continuum damage in the creep rupture of notched bars. Phil Trans R Soc Lond A 1984;311:103–129.
[5] Murakami S, Liu Y. Mesh-dependence in local approach to creep fracture. Int J Damage Mech 1995;4:230–250.
[6] He J, Sandström R. Basic modelling of creep rupture in austenitic stainless steels. Theor Appl Fract Mech 2017:89:139-146.
[7] Wen JF, Tu ST. A multiaxial creep-damage model for creep crack growth considering cavity growth and microcrack interaction. Eng Fract Mech 2014;123:197–210.
[8] Meng Q, Wang Z. Creep damage models and their applications for crack growth analysis in pipes: A review. Eng Fract Mech 2019;205:547-576.
[9] Joseph TD, McLennon D, Spindler MW, Truman CE, Smith DJ. The effect of prior cyclic loading variables on the creep behaviour of ex-service Type 316H stainless steel. Mater High Temp 2013;30:56-160.
[10] Sarkar A, Vijayanand VD, Parameswaran P, Shankar V, Sandhya R, Laha K, et al. Influence of prior fatigue cycling on creep behavior of reduced activation ferriticmartensitic steel. Metall Mater Trans A 2014;45:3023–3035.
[11] Takahashi Y. Prediction of deformation and failure of modified 9Cr–1Mo steel under creep-fatigue interaction. Mater High Temp 2012;29:280-292.

[12] Binda L, Holdsworth SR, Mazza E. Influence of prior cyclic deformation on creep properties of 1CrMoV. Mater High Temp 2010;27:21-27.
[13] Zhang W, Wang XW, Li X, Gong JM, Wahab MA. Influence of prior low cycle fatigue on microstructure evolution and subsequent creep behavior. Int J Fatigue 2018;109:114-125.
[14] Auzoux Q, Allais L, Caës C, Girard B, Tournié I, Gourgues AF, Pineau A. Intergranular damage in AISI 316L (N) austenitic stainless steel at 600 °C: Pre-strain and multiaxial effects. Nucl Eng Des 2005;235:2227-2245.
[15] Erinosho TO, Venkata KA, Mostafavi M, Knowles DM, Truman CE. Influence of prior cyclic plasticity on creep deformation using crystal plasticity modelling. Int J Solids Struct, 2018;139:129-137.
[16] Zhang W, Wang XW, Gong JM, Jiang Y, Huang X. Experimental and simulated characterization of creep behavior of P92 steel with prior cyclic loading damage. J Mater Sci Technol 2017;33:1540–1548.
[17] Oruganti R, Karadge M, Swaminathan S. Damage mechanics-based creep model for 9–10% Cr ferritic steels. Acta Mater 2011;59:2145-2155.
[18] Dyson B. Use of CDM in materials modeling and component creep life prediction. Journal of pressure vessel technology, 2000;122: 281-296.
[19] Semba H, Dyson B, McLean M. Microstructure-based creep modelling of a 9% Cr martensitic steel. Mater High Temp 2008;25:131-137.
[20] Zhang W, Wang XW, Chen HF, Zhang TY, Gong JM. Evaluation of the effect of various prior creep-fatigue interaction damages on subsequent tensile and creep properties of 9%Cr steel. Int J Fatigue 2019;125:440-453.
[21] Shankar V, Valsan M, Rao KBS, Kannan R, Mannan S L, Pathak SD. Low cycle fatigue behavior and microstructural evolution of modified 9Cr–1Mo ferritic steel. Mater Sci Eng, A 2006;437:413-422.
[22] Vogler S, Blum W. In: Wilshire B, Evans RW, editors. Creep and fracture of engineering materials and structures. London: The Institute of Metals 1990:65–79.
[23] Pandey C, Mahapatra MM, Kumar P, Saini N. Effect of normalization and tempering on microstructure and mechanical properties of V-groove and narrow-groove P91 pipe weldments. Mater Sci Eng, A 2017;685:39-49.
[24] Nagesha A, Valsan M, Kannan R, Rao KBS, Mannan SL. Influence of temperature on the low cycle fatigue behaviour of a modified 9Cr–1Mo ferritic steel. Int J Fatigue 2002;24:1285-1293.
[25] Pandey C, Mahapatra MM, Kumar P, Saini N. Some studies on P91 steel and their weldments. J Alloy Compd 2018;743:332-364.
[26] Pešička J, Kužel R, Dronhofer A, Eggeler G. The evolution of dislocation density during heat treatment and creep of tempered martensite ferritic steels. Acta Mater 2003;51:4847-4862.
[27] Eggeler G. The effect of long-term creep on particle coarsening in tempered martensite ferritic steels. Acta Mater 1989;37:3225-3234.
[28] Fournier B, Dalle F, Sauzay M, Longour J, Salvi M, Caës C, Tournié I, Giroux PF, Kimb SH. Comparison of various 9–12% Cr steels under fatigue and creep-fatigue loadings at high temperature. Mater Sci Eng, A 2011;528:6934-6945.
[29] Chauhan A, Hoffmann J, Litvinov D, Aktaa J. High-temperature low-cycle fatigue behavior of a 9Cr-ODS steel: Part 1-pure fatigue, microstructure evolution and damage characteristics. Mater Sci Eng, A 2017;707:207-220.
[30] Fournier B, Sauzay M, Barcelo F, Rauch E, Renault A, Cozzika T, et al. Creep-fatigue interactions in a 9 Pct Cr-1 Pct Mo martensitic steel: part II. Microstructural evolutions. Metall Mater Trans A 2009;40:330-341.
[31] Sauzay M, Fournier B, Mottot M, Pineau A, Monnet, I. Cyclic softening of martensitic steels at high temperature—Experiments and physically based modelling. Mater Sci Eng, A 2008;483:410-414.
[32] Barrett RA, O'Donoghue PE, Leen SB. A physically-based constitutive model for high temperature microstructural degradation under cyclic deformation. Int J Fatigue 2017;100:388-406.

[33] Ennis PJ, Zielinska-Lipiec A, Wachter O, Czyrska-Filemonowicz A. Microstructural stability and creep rupture strength of the martensitic steel P92 for advanced power plant. Acta Mater 1997;45:4901-4907.
[34] Brillet H. Comportement en Fatigue d'un Acier a` 9 Pct Cr a 550 °C. Note Technique CEA/DEN/DMN/SRMA 2003–2525, CEA, Saclay, France, 2003.
[35] Chauhan A, Hoffmann J, Litvinov D, Aktaa J. High-temperature low-cycle fatigue behavior of a 9Cr-ODS steel: part 2-hold time influence, microstructural evolution and damage characteristics. Mater Sci Eng, A 2018;730:197-206.
[36] Saini N, Pandey C, Mahapatra MM. Characterization and evaluation of mechanical properties of CSEF P92 steel for varying normalizing temperature. Mater Sci Eng, A 2017;688:250-261.
[37] Rojas D, Garcia J, Prat O, Sauthoff G, Kaysser-Pyzalla AR. 9% Cr heat resistant steels: Alloy design, microstructure evolution and creep response at 650 C. Mater Sci Eng, A 2011;528:5164-5176.
[38] Sakthivel T, Vasudevan M, Laha K, Parameswaran P, Chandravathi KS, Selvi SP, Maduraimuthu V, Mathew MD. Creep rupture behavior of 9Cr–1.8 W–0.5 Mo–VNb (ASME grade 92) ferritic steel weld joint. Mater Sci Eng, A 2014;591:111-120.
[39] Barrett RA, O'Donoghue PE, Leen SB. A dislocation-based model for high temperature cyclic viscoplasticity of 9–12Cr steels. Comp Mater Sci 2014;92:286-297.
[40] Tan L, Snead L L, Katoh Y. Development of new generation reduced activation ferritic-martensitic steels for advanced fusion reactors. J Nucl Mater 2016;478:42-49.
[41] Shibata A, Nagoshi T, Sone M, Morito S, Higo Y. Evaluation of the block boundary and sub-block boundary strengths of ferrous lath martensite using a micro-bending test. Mater Sci Eng, A 2010;527:7538-7544.
[42] Rice J R. Constraints on the diffusive cavitation of isolated grain boundary facets in creeping polycrystals[J]. Acta Mater 1981, 29(4): 675-681.
[43] Wen JF, Srivastava A, Benzerga A, Tu ST, Needleman A. Creep crack growth by grain boundary cavitation under monotonic and cyclic loading. J Mech Phys Solids 2017;108:68-84.
[44] Hu JD, Xuan FZ, Liu CJ. A void growth model of multiaxial power-law creep rupture involving the void shape changes. Int J Mech Sci 2018;144:723-730.
[45] Zhang Z, Hu Z, Schmauder S, Mlikota M, Fan K. Low-cycle fatigue properties of P92 ferritic-martensitic steel at elevated temperature. J Mater Eng Perform 2016;25:1650-1662.
[46] Kowalewski ZL, Hayhurst DR, Dyson BF. Mechanisms-based creep constitutive equations for an aluminium alloy. J Strain Anal Eng 1994;29:309-316.
[47] Mustata R, Hayhurst DR. Creep constitutive equations for a 0.5 Cr 0.5 Mo 0.25 V ferritic steel in the temperature range 565° C–675° C. Int J Press Vessel Pip 2005;82:363-372.
[48] Abe F, Nakazawa S, Araki H, Noda T. The role of microstructural instability on creep behavior of a martensitic 9Cr-2W steel. Metall Mater Trans A 1992;23:69-477.
[49] Gopinath K, Gupta RK, Sahu JK, Ray PK, Ghosh RN. Designing P92 grade martensitic steel header pipes against creep–fatigue interaction loading condition: damage micromechanisms. Mater Des 2015;86:411-420.
[50] Zhang SL, Xuan FZ. Interaction of cyclic softening and stress relaxation of 9–12% Cr steel under strain-controlled fatigue-creep condition: experimental and modeling. Int J Plast 2017;98:45-64.
[51] Yao HT, Xuan FZ, Wang Z, Tu ST. A review of creep analysis and design under multi-axial stress states. Nucl Eng Des 2007;237:1969-1986.
[52] Masuyama F. Creep rupture life and design factors for high-strength ferritic steels. Int J Press Vessel Pip 2007;84:53-61.
[53] Nikbin K. A unified multiscale ductility exhaustion based approach to predict uniaxial, multiaxial creep rupture and crack growth. Eng Fract Mech 2017;179:240-259.